Solid Earth Discuss., 6, 1579–1624, 2014
www.solid-earth-discuss.net/6/1579/2014/
doi:10.5194/sed-6-1579-2014

Solid Earth
Discussions
Open Access

A lithosphere-scale structural model of the Barents Sea and Kara Sea region

P. Klitzke[1,2], J. I. Faleide[3], M. Scheck-Wenderoth[1,2], and J. Sippel[1]

[1]Helmholtz Centre Potsdam, GFZ German Research Centre for Geosciences, Potsdam, Germany
[2]RWTH Aachen, Germany
[3]Department of Geosciences, University of Oslo, Oslo, Norway

Received: 27 May 2014 – Accepted: 2 June 2014 – Published: 10 July 2014

Correspondence to: P. Klitzke (klitzke@gfz-potsdam.de)

Published by Copernicus Publications on behalf of the European Geosciences Union.

Abstract

The Barents Sea and Kara Sea region as part of the European Arctic shelf, is geologically situated between the Proterozoic East-European Craton in the south and early Cenozoic passive margins in the north and the west. Proven and inferred hydrocarbon resources encouraged numerous industrial and academic studies in the last decades which brought along a wide spectrum of geological and geophysical data. By evaluating all available interpreted seismic refraction and reflection data, geological maps and previously published 3-D-models, we were able to develop a new lithosphere-scale 3-D-structural model for the greater Barents Sea and Kara Sea region. The sedimentary part of the model resolves four major megasequence boundaries (earliest Eocene, mid-Cretaceous, mid-Jurassic and mid-Permian). Downwards, the 3-D-structural model is complemented by the top crystalline crust, the Moho and a newly calculated lithosphere-asthenosphere boundary (LAB). The thickness distribution of the main megasequences delineates five major subdomains differentiating the region (the northern Kara Sea, the southern Kara Sea, the eastern Barents Sea, the western Barents Sea and the oceanic domain comprising the Norwegian-Greenland Sea and the Eurasia Basin). The vertical resolution of five sedimentary megasequences allows comparing for the first time the subsidence history of these domains directly. Relating the sedimentary structures with the deeper crustal/lithospheric configuration sheds some light on possible causative basin forming mechanisms that we discuss.

The newly calculated LAB deepens from the typically shallow oceanic domain in three major steps beneath the Barents and Kara shelves towards the West-Siberian Basin in the east. Thereby, we relate the shallow continental LAB and slow/hot mantle beneath the southwestern Barents Sea with the formation of deep Paleozoic/Mesozoic rift basins. Thinnest continental lithosphere is observed beneath Svalbard and the NW Barents Sea where no Mesozoic/early Cenozoic rifting has occurred but strongest Cenozoic uplift and volcanism since Miocene times. The East Barents Sea Basin is underlain by a LAB at moderate depths and a high-density anomaly in the lithospheric

mantle which follows the basin geometry and a domain where the least amount of late Cenozoic uplift/erosion is observed. Strikingly, this high-density anomaly is not present beneath the adjacent southern Kara Sea. Both basins share a strong Mesozoic subsidence phase whereby the main subsidence phase is younger in the South Kara Sea Basin.

1 Introduction

Though of increasing economic relevance, intra-continental basins are poorly understood in terms of processes controlling their evolution (Allen and Allen, 2013; Cloetingh and Burov, 2011; Gac et al., 2013; Heine et al., 2008). To comprehend the influence of possible causative subsidence mechanisms as mentioned by Heine et al. (2008), the present-day lithosphere-scale structural configuration needs to be assessed. Essential progress can be made by integrated 3-D-models. Such models can be used as a base for structural analysis but also to constrain the distribution of physical properties and their impact on different processes.

The Barents Sea and Kara Sea region is situated in such an intra-continental setting bordered by the ancient East-European Craton in the southeast and two young passive margins in the north and in the west (Fig. 1a). This region has experienced a manifold tectonic history involving multiple orogenies, episodes of intense subsidence and young continental break-up. Thereby, the orogenies are assumed to locally have set the structural grain of the deeper lithosphere which entailed different types of basin formation. Because of the assumed potential for hydrocarbon resources, this geodynamically complex setting of the Barents Sea and Kara Sea region has been in the focus of both academic and industry-driven studies for decades which have contributed to the accumulation of a large geophysical database.

Recent studies made significant progress in integrating data for larger parts of the Barents Sea. These studies focused either on the sedimentary succession (Clark et al., 2013; Henriksen et al., 2011b), the crystalline crust (Marello et al., 2013; Ritzmann et al., 2007) or encompass only parts of the Barents Sea and Kara Sea region (Barrère et al., 2009; Breivik et al., 2003, 2005; Glørstad-Clark et al., 2010; Hauser et al., 2011; Levshin et al., 2007; Piskarev and Shkatov, 2012; Ritzmann and Faleide, 2009). Consequently, there is only limited knowledge about spatial correlations between the thickness configuration of the sedimentary succession, the crystalline crust and the lithospheric mantle as well as the extent of possible lithospheric domains for the greater Barents Sea and Kara Sea region.

In the frame of this study, we aim to integrate all publicly available geological and geophysical data (from the Norwegian and Russian parts of the shelf) into a lithosphere-scale regional 3-D model that resolves the first-order characteristics of the sedimentary fill, the crystalline crust and the lithospheric mantle. Subsequently, we analyse how far characteristics of the 3-D structural model provide new insights on the relation between these different depth levels. In particular, the variations of sedimentary thicknesses (subdivided into megasequences reflecting the main geological episodes) over the entire region are integrated for the first time and discussed in the context of regional geodynamics.

2 Geological setting

The tectonic evolution of the Barents Sea and Kara Sea region (Fig. 1a) is characterised by several orogenic phases during which different lithosphere domains were assembled (Marello et al., 2013 and references therein). The composed heterogeneous basement has experienced locally intense subsidence since Paleozoic times that gave way to the accumulation of up to 20 km thick sedimentary layers. The corresponding present-day configuration of the top crystalline crust reveals structural highs and lows of different wavelengths across the Barents and Kara shelf implying that different basement domains and structural grains are situated below the southwestern Barents Sea, the eastern Barents Sea, and the southern and northern Kara Sea, respectively (Figs. 1b and 2).

SED
6, 1579–1624, 2014

After the assemblage of the East European Craton (Baltica) at ca. 2.0–1.7 Ga (Bogdanova et al., 2008) the first major tectonic event involving plate accretion occurred in the latest Precambrian in the course of the Timanian Orogeny (Fig. 2; Kostyuchenko et al., 2006; Roberts and Siedlecka, 2002). The Timan Range, a present-day topographic high (Fig. 1b) located in the southeast of the study area, gives proof of this collisional event. Orogeny-associated terrane accretion proceeded northeastwards from the Timan Range to the Timan Pechora Basin and is assumed to have continued northwards beneath the eastern Barents Sea as far as to the northern Kara Sea (Gee et al., 2006; Lorenz et al., 2007). Earliest sedimentation in these regions is reported as having occurred in latest Precambrian times (Ivanova et al., 2011; Lorenz et al., 2007) but the main sedimentary cover is of Early Paleozoic age (Malyshev et al., 2012, 2013).

The Caledonian Orogeny, caused by the collision between Laurentia and Baltica to form Laurussia (Late Cambrian to Silurian), affected mainly the area of the western Barents Sea. The sub-sedimentary crystalline crust beneath the southwestern Barents Sea is supposed to represent the northward continuation of the Caledonian thrusts cropping out in northern Norway (Figs. 1b and 2; Breivik et al., 2005; Gudlaugsson et al., 1998; Marello et al., 2013; Ritzmann and Faleide, 2007). The onshore fold and thrust belts compose a series of NE–SW striking nappes – a strike direction that dominates also the structural configuration of the basement beneath the southwestern Barents Sea (Faleide et al., 1993; Gudlaugsson et al., 1998; Ritzmann et al., 2007). This trend is disputed in recent studies (Gernigon and Brönner, 2012; Gernigon et al., 2014). However, beneath the Carboniferous rift sediments there are also assumed considerable amounts of Devonian strata deeply buried in parts of the southwestern Barents Sea (Fig. 2; Gudlaugsson et al., 1998; Ritzmann and Faleide, 2007). However, the oldest sediments found in the depressions of the southwestern Barents Sea at present-day result from post-Caledonian rifting in late Carboniferous-Permian times and gave way to the formation of e.g. the Nordkapp Basin and the Ottar Basin (Fig. 2; Gudlaugsson et al., 1998; Ritzmann and Faleide, 2007). Gernigon et al. (2014) interpret oldest

SED
6, 1579–1624, 2014

meta-sedimentary rocks in the Nordkapp Basin and on the Bjarmeland Platform even as latest Mesoproterozoic to Neoproterozoic age.

The last major orogenic phase affecting larger parts of the Barents Sea and Kara Sea, i.e. the Uralian Orogeny, was initiated by the collision of Laurussia with Siberia and Kazakhstan in Late Devonian to Late Permian times (Fig. 2; Otto and Bailey, 1995; Puchkov, 2009; Steer et al., 1998). Traces of corresponding compressional deformation are evident in the Uralian orogen and as a present-day topographic high which continues structurally along the Pai–Khoi–Novaya Zemlya fold-and-thrust-belts and in the Taimyr region in the northeast of the study area (Fig. 1b). In Late Triassic to Early Jurassic (post-Uralian) times, Novaya Zemlya was finally upthrusted and the Taimyr region experienced further crustal shortening. This westward curved fold-and-thrust belt structurally delimits the southern Kara Sea (Fig. 1b) whereby the curvature is assumed to originate from a pre-collisional embayment of Laurussia (Scott and Howard, 2010).

Another tectonic event at the Permian-Triassic transition was the magmatic activity associated with the eruption of the Siberian Traps. Traces of this event are found directly eastwards of the southern Kara Sea in the West Siberian Basin as widespread flood basalts and long-lived subsidence from Middle Jurassic to Tertiary times (Figs. 1b and 2; Nikishin et al., 2002; Reichow et al., 2005; Saunders et al., 2005; Vyssotski et al., 2006).

Time-wise coinciding with these collisional and thermal events, the East Barents Sea Basin experienced major subsidence in Permian-Triassic times (Figs. 1b and 2). Several published studies discuss the nature of the observed rapid subsidence in the East Barents Sea Basin since there are no major extensional faults and thus a classical rift scenario is unlikely. Hypotheses put forward concerning possible subsidence mechanisms include (i) a foreland basin evolution (Petrov et al., 2008), (ii) multiphase extension (O'Leary et al., 2004) or (iii) lithospheric buckling (Gac et al., 2012, 2013; Semprich et al., 2010). Conversely, the oldest sediments of the South Kara Sea Basin are assumed to have accumulated in response to rifting in the Late Permian to Middle

SED
6, 1579–1624, 2014

Triassic followed by a post-rift thermal phase lasting until late Cenozoic times (Nikishin et al., 2011).

In Middle Jurassic to Early Cretaceous times intense rifting occurred in the south-western Barents Sea (Figs. 1b and 2b; Faleide et al., 1993, 2008). Thereby, the location of maximum subsidence shifted westwards with respect to the older (Carboniferous and Late Permian-Triassic) basins and resulted in the development of the deep Tromsø Basin, the Sørvestsnaget Basin and the Bjørnøya Basin (Fig. 1b). A renewed westward shift in the locus of rifting took place in Late Cretaceous to Paleocene times and resulted in the deposition of thick sedimentary sequences in the Sørvestsnaget Basin and the Vestbakken Volcanic Province along the mainly sheared western Barents Sea margin (Faleide et al., 1993, 2008).

Continental breakup of the Norwegian-Greenland Sea and the Eurasia Basin started in late Paleocene to earliest Eocene times (Figs. 1b and 2; Faleide et al., 2008). Thereby, the Norwegian-Greenland Sea opened gradually northwards along a megashear system which constituted a structural link to the Eurasia Basin. The Fram Strait, the oceanic gateway between the two oceans, opened in mid-Miocene times (Engen et al., 2008).

In the Pliocene-Pleistocene large areas of the Barents Shelf experienced uplift and glacial erosion (Fig. 2; Dimakis et al., 1998; Dörr et al., 2012; Faleide et al., 1996; Green and Duddy, 2010; Henriksen et al., 2011a; Sobolev, 2012). As a consequence, huge submarine fans (trough-mouth fans) evolved in the adjacent oceanic-crustal domains along the western and northern passive margins (Fig. 1b; Knies et al., 2009).

3 Model construction

To investigate the greater Barents Sea/Kara Sea region (Fig. 1b) on the scale of the entire lithosphere, we have integrated multidisciplinary data such as well information, interpreted seismic refraction and reflection data, geological maps and published 3-D-models (Table A1). Since most public data were only available as bitmap information, ArcGIS 10 (Esri) was used to georeference such datasets into a consistent coordinate system (UTM 35N). The georeferenced maps and profiles were imported and compiled with other available data using Petrel 2011.1 (Schlumberger), where the georeferencing was rechecked for accuracy. After having identified the main geological units, the respective scattered data for each surface were interpolated using earthVision 8.0 (Dynamic Graphics, INC) using the Minimum Tension Gridding algorithm. Thereby, available vertical fault sets for the Mesozoic and Paleozoic surfaces were considered as vertical interpolation barriers (Fig. B1; Faleide et al., 1993; Gudlaugsson et al., 1998). The resulting interpolated surfaces were again visually compared to seismic profiles and potentially corrected when disagreeing with observations or when intersecting with other surfaces.

The continent-ocean boundary (COB) is defined as coinciding with the maximum horizontal Bouguer gravity gradients in the study area (Fig. 1b; Breivik et al., 1999; Minakov et al., 2012a). This is supported by a number of seismic reflection and refraction profiles crossing the continent-ocean transition (Breivik et al., 2003; Czuba et al., 2011; Ljones et al., 2004; Ritzmann et al., 2002, 2004; Voss and Jokat, 2007; Voss et al., 2009). The final 3-D structural model extends over 2400 km in W–E and 2180 km in N–S direction (Fig. 1b) with a horizontal grid spacing of 5 km and a vertical resolution corresponding to the number of geological units differentiated.

3.1 Construction of the crustal configuration

Glørstad-Clark et al. (2011) and Clark et al. (2013) subdivided the Phanerozoic sedimentary succession in the western Barents Sea using a seismic sequence stratigraphic approach. As a result, the authors were able to determine first-order sequences, so-called megasequences, separated by distinct unconformities. These unconformities either represent erosional surfaces or separate differently deformed sedimentary units. In the frame of this study, we used this sedimentary subdivision in order to differentiate the sedimentary cover of the entire Barents Sea and Kara Sea region even if we know that the various regions have had different evolution particularly in the Paleozoic,

SED
6, 1579–1624, 2014

which is grouped into one sedimentary megasequence. Therefore, we reviewed and evaluated all available published well and seismic data and traced the megasequence boundaries carefully across the entire study area (Table A1; Faleide et al., 1993; Henriksen et al., 2011b; Ivanova et al., 2011; Johansen, 1992). Even though the data differ significantly in their underlying methodical approach, focus, data resolution and size of the studied area, they comprise depth information on at least one of the mentioned megasequence boundaries. Consequently, we were able to model the depth configuration of the earliest Eocene, the mid-Cretaceous, the mid-Jurassic and the mid-Permian megasequence boundaries (Fig. 1b, Table A1). The base of the sedimentary succession is equivalent to the top of the crystalline crust as constrained by data from e.g. Hauser et al. (2011), Johansen et al. (1993) and Ritzmann et al. (2007). The bathymetry/topography (IBCAO 3.0; Fig. 1b; Jakobsson et al., 2012), the four megasequence boundaries and the top crystalline crust were used to calculate the thickness distributions of five megasequences (Fig. 2). Thereby, subtraction of successive depth levels disclosed inconsistencies of the 2-D interpolated surfaces due to intersections. Such intersections were encountered in particular in the southwestern Barents shelf, where large-offset faults are present. To obtain a consistent 3-D-structural model, spatial intersections were corrected which entailed a renewed cross-check with the input data. In regions where a megasequence is absent due to non-deposition or erosion, the subtracted base of the megasequence was set equal to the overlying top.

Analogously, the thickness of the crystalline crust has been calculated as the difference between the surfaces of the top crystalline crust and the crust-mantle boundary (Moho) as derived from velocity data (e.g. Hauser et al., 2011; Ivanova et al., 2011; Ritzmann et al., 2007).

3.2 Modelling of the Upper Mantle Configuration

The lithospheric thickness is an important parameter required if tectonic processes are studied since the lithosphere-asthenosphere boundary (LAB) is assumed to represent the rheological transition between the rigid lithosphere where heat transport is mainly

SED
6, 1579–1624, 2014

conductive to the underlying convection-dominated viscous asthenosphere (Turcotte and Schubert, 2002). Possible factors controlling the viscosity decrease at the LAB are e.g. temperature, water content, chemical composition and partial melts (Fischer et al., 2010; Karato, 2012). Accordingly, the nature of the LAB is discussed extensively in literature (Eaton et al., 2009; Fischer et al., 2010; Karato, 2012 and references therein). Particularly, partial melting is described to possess the potential to reduce the viscosity significantly even if occurring only in small amounts (Fischer et al., 2010). Shear-wave velocities are a well-suited parameter to monitor such viscosity changes and hence, partial melting (Fischer et al., 2010). To assess the configuration of the lithospheric mantle and to derive information on the depth position of the LAB, we have analysed published shear-wave velocity models based on surface wave tomography (Levshin et al., 2007; Shapiro and Ritzwoller, 2002).

The regional BARMOD dataset (Levshin et al., 2007) is a 3-D grid with a horizontal resolution of 50 km and 5 km in vertical direction. This grid comprises information on the 3-D shear-wave velocity distribution for large parts of the upper mantle beneath the Barents Sea and northernmost Scandinavia, Novaya Zemlya, Svalbard, Franz Josef Land and the western parts of the southern Kara Sea (Fig. 5c). In the oceanic domain, the extent of BARMOD is restricted to the eastern part of the Norwegian-Greenland Sea. Vertically, BARMOD reaches down to a maximum depth of −250 km.

As the easternmost continental parts of the study area are not covered by the BARMOD dataset, we used the global dataset CUB1.0 by Shapiro and Ritzwoller (2002) as a source of information on the mantle shear-wave velocity configuration for this region. This complementary dataset has a horizontal resolution of 2° and a vertical resolution of 4 km.

Both, the BARMOD and CUB1.0 datasets show mantle shear-wave velocities that decrease with increasing depth over a certain depth interval. This zone laterally varies in thickness and depth. We have determined the depth range of this zone of reduced shear velocities for each XY-position of the 3-D velocity models by calculating the differences in shear-wave velocities (Δv_s) between pairs of vertically adjacent grid nodes.

SED
6, 1579–1624, 2014

Therefore, the shear wave velocity of a grid node located at shallower depth, z1, is subtracted from a grid node at larger depth, z2, respectively:

$$\Delta v_s = v_{s,z2} - v_{s,z1} \quad (1)$$

Accordingly, the 3-D geometry of the mantle zone where a velocity inversion with depth appears, is defined by grid nodes characterised by $\Delta v_s < 0$. Thus, this reduction corresponds to an inversion of the usual, mainly pressure-controlled trend of increasing velocities with increasing depth ($\Delta v_s > 0$) as evident above and below this zone of decreasing velocities. We find large lateral variations in the thickness of this zone characterised by decreasing velocities across the study area. Furthermore, Δv_s is not uniform over these depth ranges but tends to increase in magnitude from the upper and lower limits of this zone of reduced velocities towards its centre. In the central parts of this zone incremental velocity reduction values of up to $\Delta v_s = -0.02\,\mathrm{km\,s^{-1}}$ per kilometre vertical distance were obtained. We interpreted the depth where the incremental velocity reduction is greatest for an XY-position (Δv_s = minimum) as the depth at which the geotherm cuts the solidus of mantle rock to induce first significant partial melting. Hence, we mapped the depth of Δv_s = minimum over the spatial extension of BARMOD and CUB1.0 and interpret it as the depth distribution of the LAB.

In the oceanic domain, the BARMOD dataset is restricted to the easternmost part of the Norwegian-Greenland Sea and the resolution of CUB1.0 is too coarse for the narrow oceanic domain. Therefore, we were forced to find an alternative approach to derive the depth position of the LAB in the oceanic domain. Interestingly, Zhang and Lay (1999) detected a negative correlation of mid-oceanic spreading rates with recorded surface waves velocities in the Pacific, the Indian and the Atlantic Oceans. Slow mid-oceanic spreading rates, as observed in the Atlantic Ocean, are associated with slow mantle upwelling which is thought to lead to a rigidification of the mantle material at greater depths than, for example, in the fast-spreading Pacific Ocean. Deep rigidification of mantle material is also observed for the ultra-slow spreading Knipovich Ridge in the Norwegian-Greenland Sea (Dick et al., 2003; Huang and Solomon, 1988;

Sauter et al., 2011). Additionally, Zhang and Lay (1999) noticed only a minor lithospheric thickness increase in the Atlantic Ocean with increasing age of the seafloor. Based on their observations the authors set up an empirical equation to calculate the oceanic lithospheric thickness (L) as a function of age (t) for the Atlantic Ocean.

$$L = 44.6 + 0.8 \times \sqrt{t} \tag{2}$$

The Gakkel Ridge in the Eurasia Basin is, like as the Knipovich Ridge in the Atlantic Ocean, an ultra-slow spreading ridge characterised by spreading rates slower than $20\,\mathrm{mm\,a^{-1}}$ (Dubinin et al., 2013 and references therein). This justifies the application of the equation of Zhang and Lay (1999) also for the Eurasia Basin. Accordingly, we calculated the oceanic lithosphere thickness using the oceanic age grid of Müller et al. (2008). Where BARMOD extends into the oceanic domain, the depth of the determined LAB is consistent with the LAB modelled according to Zhang and Lay (1999) which again justifies the used approach.

To derive the first depth map of the LAB for the entire study area, we integrated the velocity-derived information (BARMOD, CUB), oceanic-age related depths as well as information from S-receiver functions for East Greenland (Kumar et al., 2005).

4 Results

4.1 Structure of the sedimentary infill

The bathymetry/topography (Fig. 1b) represents the uppermost surface of the 3-D structural model and shows typical shallow water depths (average of about −300 m) over the shelf, whereby single archipelagos (Novaya Zemlya, Svalbard, Franz Josef Land) elevate to more than 1000 m. The northern and western boundaries of the shelf are characterised by passive margins and a rather steep slope defining the transition to the up to −4000 m deep oceanic domain of the Norwegian-Greenland Sea and the Eurasia Basin.

SED
6, 1579–1624, 2014

The earliest Eocene interface (Fig. 3a) represents the shallowest megasequence boundary and equals the bathymetry/topography over wide parts of the continental domain. Only in the southwesternmost Barents Sea, a depression defines the transition to the oceanic domain where the earliest Eocene surface reaches depths of more than −8000 m. close to the COB. Similar depressions occur also along the northern passive margin in the Eurasia Basin. The earliest Eocene megasequence boundary in the oceanic domain is equivalent to the top of the crystalline crust. According to the depth differences between the bathymetry/topography and the earliest Eocene surface, the thickness distribution of the earliest Eocene–present sediments show thickness maxima mostly restricted to the oceanic domain (up to 7500 m) whereas no deposits of this age appear in most of the continental domain apart from the southwesternmost Barents Sea (Fig. 4a).

The mid-Cretaceous megasequence boundary (Fig. 3b) reveals minor depressions in the South Kara Sea Basin, in the West Siberian Basin, in the southern part of the East Barents Sea Basin and is more markedly in the western Barents Sea (Sørvestsnaget Basin, Vestbakken Volcanic Province). Accordingly, these basins exhibit the largest depth differences between the mid-Cretaceous and the overlying earliest Eocene surface, which is clearly outlined in the calculated thickness distribution of the mid-Cretaceous–earliest Eocene megasequence (Fig. 4b). Within the southern Kara Sea a mid-Cretaceous–earliest Eocene depocentre reveals a prominent N–S trend. The sub-basins of the western Barents Sea, on the other hand, depict different strike directions of thickness maxima ranging from N–S in the west (Vestbakken Basin) to rather ENE–WSW in the east (Hammerfest and Nordkapp Basins). Thereby, the wavelength of thickness variations is much shorter in the western Barents Sea than across the remaining study area. These pronounced thickness variations in the western Barents Sea reflect the structural effect of offsets along relatively closely spaced faults (see Mesozoic faults in Fig. B1).

The mid-Jurassic and the mid-Permian megasequence boundaries (Fig. 3c and d) show similar geometries as the overlying mid-Cretaceous surface with narrow and deep

SED
6, 1579–1624, 2014

depressions in the western Barents Sea and rather wide depressions in the East Barents Sea and the South Kara Sea. The corresponding sediments of the mid-Jurassic–mid-Cretaceous megasequence attain thicknesses of up to about 11 000 m in the western Barents Sea within a N–S to NE–SW fan-shaped structure (Fig. 4c and d). Further east in the East Barents Sea Basin and the South Kara Sea Basin, the mid-Jurassic–mid-Cretaceous unit is characterised by moderate thicknesses (< 3000 m) arranged in a bowl-shaped geometry following the curvature of Novaya Zemlya.

The underlying mid-Permian–mid-Jurassic sediment maxima are similar in shape and orientation axes but are considerably thicker in the basins of the western Barents Sea (~ 15 000 m), the eastern Barents Sea (~ 10 500 m) and southern Kara Sea (~ 6000 m; Fig. 4d).

The deepest megasequence overlying the top of the crystalline crust is the pre-mid-Permian megasequence (Fig. 4e) which encompasses numerous small-scale thickness maxima which are mainly related to the topography of the top crystalline crust (Fig. 4f). The western Barents Sea is marked by rather thin pre-mid-Permian sediments while they attain up to ~ 10 000 m in the northern part of the Kara Sea and in the East Barents Sea Basin.

The top of the crystalline crust (Fig. 4f) is divided by the COB (continent-ocean boundary) into an oceanic and a continental domain (Fig. 1b). In the oceanic domain, the top crystalline crust is modelled as being identical with all megasequence boundaries, since the oceanic crust is younger than the youngest megasequence boundary in the model (Fig. 2).

In the continental domain, the top of the crystalline crust reveals significant depth variations (Fig. 4f), especially across the wide shelf areas though the bathymetry is rather uniform (Fig. 1b). Given this flatness of the top of the sediments and the consistency of the 3-D structural model, the depth variations of the crystalline crust directly reflect the cumulative thickness variations of the sedimentary megasequences. Accordingly, depressions of the top crystalline crust correlate with domains of larger sediment thickness. The deepest depressions of the top crystalline crust descend down to

SED
6, 1579–1624, 2014

−14 000 m in the northern and southern Kara Sea and to almost −20 000 m in the East Barents Sea Basin and in the western Barents Sea. The distance between basement highs and lows is considerably smaller in the western Barents Sea (< 100 km) compared to the East Barents Sea Basin and Kara Sea basins (∼ 500 km). The eastern Barents Sea and the Kara Sea are both subdivided into two subbasins separated by structural highs of the crystalline crust (Fig. 4f). Thereby, the prominent structural high separating the northern and southern Kara Sea follows the topographic highs formed by the Ural mountain chain, the Pai–Khoi–Novaya Zemlya fold-and-thrust belts and the Taimyr region (cf. Fig. 1b).

4.2 Crust and mantle structure

The depth map of the Moho illustrates a stepwise W–E deepening structure (Fig. 5a) with shallowest depths beneath the oceanic domain (< −15 km), moderate depths beneath the shelf (−35 km) and largest depths beneath the continental mainland (< −50 km). Moreover, the Moho is essentially shallower (−24 km) beneath regions situated close to the COB and NW of Svalbard (Fig. 1b). Beneath the East Barents Sea Basin and the northern Kara Sea, the Moho topography is flat at −30 km even below prominent sediment maxima (cf. Fig. 4d and e). The South Kara Sea Basin is underlain by a Moho at similar depths as the North Kara Sea, but is deepening towards the Ural Orogen in the south, Novaya Zemlya in the west and Taimyr Peninsula in the north (−50 km). Consequently, the crystalline crust is thickest below the foldbelts and towards the continental shield area (Fig. 5b). Below the shelf, the crystalline crust is moderately thick (locally up to 33 km) and thinned below regions covered by the thickest sediments (SW Barents Sea basins, East Barents Sea Basin, South Kara Sea Basin). The oceanic domain is defined by typical crustal thicknesses of 7 km.

As found for the Moho, also the modelled LAB exhibits a comparable step-like W–E deepening with a shallow oceanic LAB (−55 km), a depth range from −60 to −155 km beneath the Barents Sea and the largest depths beneath the Kara Sea and the continental mainland (down to −200 km; Fig. 5c). Thereby, wider domains of a rather flat

LAB alternate with narrower domains of steep depth gradients. Accordingly, the thickness distribution of the lithospheric mantle thickness follows the described W–E trend of the LAB relief. The thinnest lithospheric mantle is found below the oceanic domain, the westernmost Barents Sea and Svalbard. Beneath the shelf, the lithospheric mantle is thickening successively from west to east below the East Barents Sea Basin and beneath Novaya Zemlya. The Kara Sea and the continental domain are underlain by largest lithospheric mantle thicknesses (Fig. 5d). Also recently published LAB maps show the trend of an shallow LAB beneath Svalbard and a strong deepening towards the Barents Shelf and the continental mainland, though the absolute depths vary significantly between these models (Gung et al., 2003; Koptev and Ershov, 2011; McKenzie and Priestley, 2008; Priestley and McKenzie, 2006).

The integrated structural configuration of the entire lithosphere, including the sedimentary megasequences, the crystalline crust, and also the shear wave velocity distribution of the mantle is illustrated on the basis of five profiles (Fig. 6) that cross representative domains of the Barents Sea and Kara Sea region (for location see Fig. 1b). The W–E profiles (Fig. 6a–c and e) demonstrate the eastward stepwise deepening of the Moho and the LAB showing no significant correlation with structural changes in the sedimentary basins. Following the mantle shear wave velocities in the same eastward direction, a distinctive increase of velocities is observable from the oceanic towards the continental domain with highest velocities beneath the eastern Barents Sea. The N–S profile (Fig. 6d) illustrates the generally deeper Moho beneath the continental mainland and the distinct shallowing below the South Kara Basin, while the LAB is only shallowing below the northern Kara Sea and towards the oceanic domain in the northernmost part.

5 Discussion

The 3-D structural model allows analysing sedimentary units according to their stratigraphic ages. Thus, the different thickness maxima of the sedimentary units can ten-

SED
6, 1579–1624, 2014

tatively be interpreted in terms of depositional centres and associated subsidence patterns by regarding also the configuration of the crystalline crust and of the lithospheric mantle. These spatial correlations, in turn, may shed new light on large-scale tectonic mechanisms accompanying the main geodynamic events.

It is well known that the lithosphere amalgamated successively by terrane accretion processes during the Timanian, Caledonian and Uralian orogenies. Strikingly, the LAB depth configuration also outlines regions which are at comparable depth but separated by large depth gradients (Fig. 5d). Hence, we may interpret the present-day separation of the Barents and Kara Sea region into domains of differently thick lithosphere as indicating paleo-terranes having been affiliated in the course of these orogenies.

Marello et al. (2013) describes such domains for the crystalline crust on the basis of gravity and magnetic anomalies. The authors were able to differentiate eleven basement terranes according to the Timanian, the Caledonian and Uralian orogenies and additional Pre-Carboniferous basement blocks. By simplifying the classification of Marello et al. (2013) to four major basement terranes which correspond to the three orogenies and a Barentsia crustal block (Fig. 7), we find major correlation between the basement terranes of Marello et al. (2013) and the lithospheric thickness structure of our model.

The thin continental lithosphere beneath the western/central Barents Sea (60 km to 105 km) coincides with the Caledonian basement (southwest) and the Barentsia crustal block (northwest) described by Marello et al. (2013) (Fig. 7). Thereby, the local lithospheric thickness configuration allows no clear differentiation of these two basement blocks in the western Barents Sea. Beneath the eastern Barents Sea, the lithosphere forms a narrow domain of similar thicknesses (~ 150 km) which correlates with the Timanian basement of Marello et al. (2013) though the latter is much wider (Fig. 7). The west coast of Novaya Zemlya represents the boundary to the Uralian domain (Fig. 7) on crustal-scale (Marello et al., 2013) as well as on lithosphere-scale (lithosphere thickness: 180 km to 195 km). However, there are local differences between crustal and lithosphere thickening trends e.g. in the area south and southwest of Novaya Zemlya

SED
6, 1579–1624, 2014

(Timan-Pechora region; cf. Figs. 5b, d and 7) which indicates less well defined terrane boundaries. Accordingly, Marello et al. (2013) described the crustal part of the Timan-Pechora region as a transitional/reworked Timanian/Uralian domain which could explain why the lithospheric thickening is not correlating perfectly with the Uralian crustal root. This applies also for the boundary between the Caledonian and Timanian terrane in the central Barents Sea.

5.1 Pre-mid-Permian

The pre-mid-Permian sedimentary strata constitute the lowermost megasequence which overlays directly the crystalline crust. It has to be noted that the age of basal sediments within the pre-mid-Permian megasequence varies distinctively laterally beneath the Barents Sea and Kara Sea region according to different basement/lithospheric domains and the onset of subsidence as outlined in the geological setting. The differentiation of such deep and old sedimentary rocks from the underlying crystalline crust using seismic imaging techniques alone is challenging. The large depths involve, beside a compaction-induced density increase, also elevated pressure and temperature conditions which enforce diagenesis and enable low-grade metamorphism. As a result, the seismic velocities may be increased and the acoustic impedance between sediments and crystalline crust reduced. This hampers the detectability of sediment-characteristic structures (e.g. stratification) in seismic data which in turn could favour misinterpretation of corresponding reflectors as top crystalline crust. Beside the property-induced impedance decrease, also high-velocity rocks such as salt (e.g. SW Barents Sea) or intrusive volcanics (e.g. East Barents Sea Basin, Svalbard, Timan-Pechora Basin, West-Siberian Basin) aggravate the distinction between sediments and crystalline crust (Artyushkov, 2005; Breivik et al., 2005; Gee et al., 2000; Ivanova et al., 2011; Vyssotski et al., 2006). This may connote locally an underestimation of the pre-mid-Permian sedimentary thickness and an overestimation of the subsedimentary crustal thickness.

Despite these limitations and uncertainties, the thickness map of the pre-mid-Permian sediments shows reproducible trends as e.g. in the northern Kara Sea where

SED
6, 1579–1624, 2014

a NW-striking sediment maximum attains a thickness of up to 12 500 m (Fig. 3e). This thickness maximum is oriented almost perpendicular to the prevailing structural orientation of the Barents and Kara shelf where Caledonian and Uralian structural features strike NE–SW and N–S, respectively. Towards the south and the southwest, the pre-mid-Permian sediments are bounded by two structural highs of the crystalline crust (Figs. 1b, 3f and 6c and d). The NW–SE orientation of the crustal high separating the eastern Barents Sea and the northern Kara Sea correlates with the interpreted Timanide suture of the North Kara plate which is assumed to have accreted during the Timanian Orogeny in the latest Precambrian (Cocks and Torsvik, 2005; Lorenz et al., 2007). This may have caused the formation of the NW-striking thickened crust and of the sedimentary basin in the hinterland (Fig. 1b; (Malyshev et al., 2012a). Conversely, the Moho and the LAB are rather flat below the northern Kara Sea and show no characteristic structure (Fig. 5a and c). This indicates that the crustal imprint of a possibly associated thinning event was vanished during later basin history or that a subsidence mechanism different from lithospheric thinning was responsible for the basin formation. However, the thickness of the lithosphere beneath the northern Kara Sea (165 km) neither fits to its southern Kara Sea (180 km to 195 km) nor to the Barents Sea (60 km to 150 km) implying the existence of a North Kara terrane (Cocks and Torsvik, 2005).

The western Barents Sea was affected essentially by the Caledonian Orogeny. Subsequently, wide parts of the western Barents Sea experienced denudation and erosion, so that larger thicknesses of Devonian-Carboniferous strata are restricted to the Hammerfest Basin and Nordkapp Basin (Fig. 4e; Gudlaugsson et al., 1998; Ritzmann and Faleide, 2007). The NE–SW to NNE–SSW striking trend of these basins is assumed to be inherited from the Caledonian Orogeny (Breivik et al., 2005; Gudlaugsson et al., 1998; Ritzmann and Faleide, 2007). Corresponding nappes and thrust sheets are well documented onshore Scandinavia and are supposed to continue beneath the western Barents Sea (Faleide et al., 1993; Gudlaugsson et al., 1998; Ritzmann and Faleide, 2007). However, in recent studies (Gernigon and Brönner, 2012; Gernigon et al., 2014)

SED
6, 1579–1624, 2014

the striking trend of the nappes and the thrust sheets in the western Barents Sea is disputed.

The eastern part of the Barents Sea is covered by a thicker pre-Devonian (up to 6 km) and a thinner Carboniferous–early Permian section (up to 2 km) (Artyushkov, 2005; Ritzmann and Faleide, 2009) which are integrated in the 3-D model into the pre-mid-Permian megasequence (Fig. 4e).

5.2 Mid-Permian to earliest Eocene

The mid-Permian to earliest Eocene interval encompasses three megasequences (mid-Permian–mid-Jurassic, mid-Jurassic–mid-Cretaceous, mid-Cretaceous–earliest Eocene). The thickness configurations of the respective megasequences show that the Barents Sea and Kara Sea region experienced significant subsidence during this time interval. Thereby, subsidence varies strongly through time in different subdomains, which can be related to certain tectonic and geodynamic developments. For example, the eastern Barents Sea and the southern Kara Sea were affected by compression until Late Triassic–Early Jurassic times in response to the Uralian Orogeny. Conversely, the western Barents Sea experienced different extensional phases from late Paleozoic to early Cenozoic times preceding the break-up of the North Atlantic. Owing to the underlying lithospheric domains (Fig. 7) and different prevalent stress fields which obviously influenced basin formation, the tectonic evolution of the eastern Barents Sea/southern Kara Sea and of the western Barents Sea are analysed separately in the following.

5.2.1 Eastern Barents Sea/Southern Kara Sea

The main part of the preserved sedimentary succession in the East Barents Sea Basin corresponds to the mid-Permian–mid-Jurassic megasequence while the two overlying megasequences are distinctively thinner (mid-Jurassic–mid-Cretaceous, mid-Cretaceous–earliest Eocene; Fig. 4b–d). The pre-mid-Jurassic sediment configuration in the southern Kara Sea is less well constrained due to a lack of borehole data. How-

SED
6, 1579–1624, 2014

ever, seismic profiles (Ivanova et al., 2011; Malyshev et al., 2012b; Nikishin et al., 2011; Stoupakova et al., 2011) indicate that a significant amount of mid-Permian to mid-Jurassic sediments is present beneath the southern Kara Sea as also indicated by the model (Figs. 4c and 6b, d). The overlying megasequences (mid-Jurassic–mid-Cretaceous and mid-Cretaceous–earliest Eocene) also show decreasing thicknesses. This implies that the East Barents Sea Basin – and maybe also the southern Kara Sea – experienced strong subsidence in an early tectonic phase followed by weaker subsidence until Paleocene times. The Moho is at comparable depths below both basins (at about −33 km) but deepens substantially beneath Novaya Zemlya forming a structural boundary between the two basins (Figs. 5b and 6b).

There are also significant differences between the East Barents Sea Basin and the South Kara Sea Basin. The preserved mid-Permian–mid-Jurassic megasequence is distinctively thicker in the East Barents Sea Basin (10 500 m) compared to the South Kara Sea Basin (6500 m) (Figs. 4d and 6c) indicating stronger subsidence west of Novaya Zemlya (Figs. 4d and 6c). In contrast, for the mid-Jurassic–mid-Cretaceous and the mid-Cretaceous–earliest Eocene megasequences the amount of preserved sediments is higher in the South Kara Sea Basin (3300 m and 1700 m) than in the East Barents Sea Basin (2200 m and 600 m). This implies a general eastward shift of major subsidence over Mid-Permian to Paleocene times.

Two major geodynamic events coincide with the deposition of the mid-Permian–mid-Jurassic sedimentary megasequence in the East Barents Sea Basin and the South Kara Sea Basin. The first event, the Uralian Orogeny, is preserved as a present-day topographic high in concert with a deep Moho along the northern Ural Mountains, the Pai–Khoi–Novaya Zemlya fold-and-thrust belts and the Taimyr region (Figs. 1b, 2 and 6b; Echtler et al., 1998; Puchkov, 2009). The second geodynamic event corresponds to the eruption of flood basalts forming the Siberian Traps at the Permian-Triassic boundary (Cherepanova et al., 2013 and references therein, Figs. 1b and 2). Widespread eruption of flood basalts due to rise of a mantle plume is held responsible to have induced Middle Jurassic to Tertiary thermal subsidence of the West-Siberian Basin

SED
6, 1579–1624, 2014

(Cherepanova et al., 2013; Vyssotski et al., 2006). The proximity of the East Barents Sea Basin and the southern Kara Sea to the Uralian orogenic root, the West Siberian Basin and the major subsidence during the mid-Permian–mid-Jurassic time interval points a close link between the basin formation and these two geodynamic events (chapter 2).

For the East Barents Sea and South Kara Sea Basin, numerous subsidence mechanisms were postulated in recent years. They include among others (i) a foreland basin evolution (Petrov et al., 2008), (iii) multiphase extension (Ivanova et al., 2006; O'Leary et al., 2004) or (iii) lithospheric buckling (Gac et al., 2012, 2013; Semprich et al., 2010). Whatever the mechanism controlling the strong Late Permian-Early Triassic subsidence, pure extension of the crust appears to be unlikely since traces of pronounced extension in the form of corresponding large normal faults and strong crustal thinning are absent in the basin (e.g. Ivanova et al., 2011; Khutorskoi et al., 2008).

A mechanism that might explain the development of the East Barents Sea Basin is lithospheric buckling that has been discussed also for other basins (Cloetingh and Burov, 2011). The compressional stress due to the Uralian Orogeny, could have induced folding of the lithosphere, which may have involved densification of the fertile and mafic lower crust and lead to the strong observed subsidence in in Late Permian-Early Triassic times (Gac et al., 2012, 2013; Semprich et al., 2010). An important observation is the spatial correlation of the East Barents Sea Basin with the extent of the high shear-wave velocity anomaly in the lithospheric mantle (Fig. 6a and b; Levshin et al., 2007). The authors relate the anomaly with subduction in the course of the Caledonian and/or Uralian orogenies. On the other hand the maximum thickness of the high-velocity anomaly coincides with the outline of the Timanian terrane (cf. Figs. 6a and 7; Ritzmann and Faleide, 2009). Whatever their origin, the high mantle velocities probably reflect higher densities which, in turn, might have caused deep-seated negative buoyancy and shallow subsidence of the East Barents Sea Basin.

In contrast to the East Barents Sea basin, there are no larger shear-wave velocity anomalies observed in the lithospheric mantle beneath the Southern Kara Sea

SED
6, 1579–1624, 2014

(Fig. 6b and d), which excludes densification of the upper mantle as a driving subsidence mechanism. An alternative mechanism is therefore needed to explain the observed mid-Permian–mid-Jurassic sediment thickness maximum here (Figs. 4d and 6a). A first subsidence stage of the southern Kara Sea is described as rifting-induced with N–S oriented graben-like structures in late Paleozoic to early Mesozoic times due to orogenic collapse (Fig. 6b; Ivanova et al., 2011; Malyshev et al., 2012b; Nikishin et al., 2011; Stoupakova et al., 2011) even though there is only little control on the pre-Jurassic stratigraphy due to a lack of deep borehole data. Furthermore, the extensional regime is hard to explain with the main compressional phase on Novaya Zemlya up to Late Triassic–Early Jurassic times (Scott and Howard, 2010). Conversely, the deep N–S striking graben-like structures in the southern Kara Sea may originate also from a transtensional regime as part of the Uralian Orogeny (Nikishin et al., 2011). Continuous seismic reflections interpreted as sedimentary layers indicate that from the mid-Jurassic on, the South Kara Sea Basin adopted a clear bowl-shaped geometry where faulting did not play a significant role for creating accommodation space (Ivanova et al., 2011). To explain the subsidence in the South Kara Sea Basin, we might have to widen the view. The mantle plume beneath the West Siberian Basin is thought to have reached also below the Southern Kara Sea basin (Saunders et al., 2005) and might thus have caused post-Permian thermal subsidence also there.

5.2.2 Western Barents Sea

In contrast to the wide and bowl-shaped structural depression of the eastern Barents Sea, the western Barents Sea is traversed by a system of structural lows and highs of the top crystalline crust (Fig. 4f) with corresponding locally thick sedimentary packages (Fig. 4a–e). These NE–SW or NNE–SSW striking narrow troughs are structurally limited by major late Paleozoic and Mesozoic normal faults that cover the entire western Barents Sea (Fig. B1).

The sediment thickness distribution indicates that rifting and hence subsidence shifted westwards with time as observable in the sedimentary megasequence which

SED
6, 1579–1624, 2014

thicken towards the west with decreasing age (Fig. 3b–e). Major rifting in the southwestern Barents Sea continued in mid-Jurassic times giving birth to deep basins (Tromsø Basin, the Sørvestsnaget Basin and the Bjørnøya Basin; Faleide et al., 1993). In the Early Cretaceous, the northern Barents Sea was uplifted related to the Arctic Large Igneous Province (Drachev and Saunders, 2006; Maher and Harmon, 2001; Minakov et al., 2012b; Smelror et al., 2009; Worsley, 2008). The uplifted areas provided a major sediment source for the subsiding basins in the southwestern Barents Sea. Late Cretaceous-Paleocene rifting resulted in the formation of pull-apart basins, and finally in break-up of the Norwegian-Greenland Sea (Faleide et al., 1993, 2008; Libak et al., 2012). The rifting history and the Caledonian affiliation is also reflected in the sub-sedimentary thickness configuration in terms of a thinned crystalline crust and lithospheric mantle (Fig. 5b and d). Besides a typical, strongly fault-related thinning of the crystalline crust below the rifted sedimentary basins, the crystalline crust is further thinning also regionally towards the COB. The slow shear wave velocities of the mantle beneath the western Barents Sea point to a lower viscosity induced by elevated temperatures, the latter probably being a relic of the young rifting history of the western Barents Sea and seafloor spreading (Fig. 6a, b and e).

5.3 Earliest Eocene to present

The Norwegian-Greenland Sea opened progressively northwards along a mega-shear system with assumed rifting in the Vestbakken Volcanic Province. This explains the clearly thinned present-day crystalline crust and lithospheric mantle in regions close to the COB (Figs. 4b, d and 6e).

In late Cenozoic times, widespread uplift affected the Barents Sea and Kara Sea region and resulted in significant erosion of the uppermost sediments particularly on Svalbard and the northwestern Barents Sea. Accordingly, youngest strata are missing across wide parts of the shelf. The timing and triggering mechanism(s) behind this uplift are still debated. Besides isostatic rebound in response to melting of thick Pliocene/Pleistocene ice sheets (Green and Duddy, 2010; Henriksen et al., 2011a), also a tectonic pulse prior to the onset of glaciations is proposed (Dimakis et al., 1998). Green and Duddy (2010) and Japsen et al. (2010) observe synchronous exhumation across wide parts of the Arctic which would require a more regional trigger.

Beneath these regions where the uplift was strongest, as on Svalbard and the northwestern Barents Sea (Dimakis et al., 1998; Green and Duddy, 2010; Henriksen et al., 2011), the modelled continental LAB is shallowest. Accordingly, Svalbard exhibits a clearly thinned continental lithospheric mantle of about 30 km (Fig. 5d). Dörr et al. (2013) state that Svalbard experienced an isostatic uplift phase around ~ 36 Ma due to magmatic underplating at the base of the crust. Referring to the authors a second uplift phase may have been induced by thinning of the lithospheric mantle beneath Svalbard which was caused by small-scale mantle convection due to adjacent seafloor spreading. The observed Miocene to recent volcanism (Dörr et al., 2013) additionally have overprinted the structural lithosphere-scale imprints of a possible Barentsia block which was assessed by Marello et al. (2013) on crustal-scale using potential field data (Fig. 7).

In contrast to the northwestern shelf edge, the eastern Barents Sea experienced rather little late Cenozoic uplift and erosion (Henriksen et al., 2011a; Sobolev, 2012). Thereby, the area affected by the least erosion correlates spatially with the outline of the East Barents Sea Basin but also with a domain where highest velocities in the lithospheric mantle (Fig. 6b and c) are observed. Consequently, the high velocities in the lithospheric mantle may have contributed not only to the formation of the East Barents Sea Basin in Paleozoic times but may have also prevented significant uplift in late Cenozoic times.

6 Summary and conclusions

We have constructed a 3-D structural model of the greater Barents Sea and Kara Sea region that resolves the first-order characteristics of its sedimentary cover, its crystalline crust as well as of its lithospheric mantle. A large amount of multidisciplinary geophysical and geological data were integrated, to model the best-possible structural configuration of the following continental subdomains: (1) the northern Kara Sea, (2) the southern Kara Sea, (3) the eastern Barents Sea and (4) the western Barents Sea.

1. The North Kara Sea Basin is covered mainly by pre-mid-Permian sediments indicate that its major subsidence phase was prior to the adjacent sedimentary basins. The sediment maximum is separated from the Barents Sea by an NW-striking thickened crystalline crust which may have originated from the late Neoproterozoic Timanian Orogeny. The depth position of the LAB may delineate the North Kara terrane.

2. The southern Kara Sea reveals a rather independent evolution from its northern counterpart. A distinctively deeper LAB delimits the sedimentary basin from the Barents Sea and northern Kara Sea and may suggests an affiliation with the Siberian plate. The South Kara Sea Basin lacks major pre-mid-Permian sediments, but has accumulated the major part of its sedimentary infill in mid-Permian to earliest Eocene times. Thereby, the younger sedimentary megasequences are thinner implying a decaying subsidence with time that was of a thermal origin and possibly related to the magmatism of the West-Siberian Mantle Plume.

3. Thickest sediments in the eastern Barents Sea have been preserved from the mid-Permian–mid-Jurassic megasequence indicating strong subsidence back then. Below the East Barents Sea Basin the LAB exhibits two major eastward deepening steps limiting a narrow zone of rather constant depth which fits neither with depths observed beneath the western Barents Sea nor to those beneath of the southern Kara Sea. Instead, this domain could be a remnant of the Timanian Orogeny which is assumed to have continued from the Timan-Pechora Basin northwards to the northern Kara Sea region. Strikingly, the sedimentary succession in the East Barents Sea Basin shows no larger extensional faults but is coinciding spatially with anomalously high shear-wave velocities/densities in the lithospheric mantle that may played an essential role during its basin evolution.

SED
6, 1579–1624, 2014

Lithospheric buckling with associated phase transitions (Gac et al., 2012, 2013; Semprich et al., 2010) could explain the intense subsidence in Permian to Triassic times, but also the elevated velocities in the lithospheric mantle. The high-density anomaly may also be responsible for less intense uplift of the eastern Barents Sea in late Cenozoic times compared to the NW Barents Sea.

4. The southwestern Barents Sea exhibits a classical rift system with major extensional faults. The amounts of sediments deposited as megasequences increase with time towards the present-day COB indicating a westward shift in rifting. The shallow Moho and LAB as well as low seismic shear wave velocities in the mantle indicating high mantle temperatures are consistent with the assumption of a rift scenario. The continental LAB is shallowest below Svalbard and the northwestern Barents Sea where late Cenozoic uplift and volcanism are observed.

Acknowledgements. We acknowledge financial support by Statoil for parts of the work reported on here. Also we would like to thank for constructive discussions with colleagues involved in the project BARMOD currently funded by the Research Council of Norway and Statoil.

The service charges for this open access publication have been covered by a Research Centre of the Helmholtz Association.

References

Allen, P. A. and Allen, J. R.: Basin Analysis: Principles and Application to Petroleum Play Assessment, 3rd edn., Wiley-Blackwell, 2013.

Artyushkov, E.: The formation mechanism of the Barents basin, Russ. Geol. Geophys.+, 46, 700–713, available at: http://www.agu.org/wps/rgg/46/46.07/articles/S02JUL05.PDF (last access: 9 May 2014), 2005.

Barrère, C., Ebbing, J., and Gernigon, L.: Offshore prolongation of Caledonian structures and basement characterisation in the western Barents Sea from geophysical modelling, Tectonophysics, 470, 71–88, doi:10.1016/j.tecto.2008.07.012, 2009.

SED

6, 1579–1624, 2014

Bogdanova, S. V., Bingen, B., Gorbatschev, R., Kheraskova, T. N., Kozlov, V. I., Puchkov, V. N., and Volozh, Y. A.: The East European Craton (Baltica) before and during the assembly of Rodinia, Precambrian Res., 160, 23–45, doi:10.1016/j.precamres.2007.04.024, 2008.
Breivik, A. J., Verhoef, J., and Faleide, J. I.: Effect of thermal contrasts on gravity modeling at passive margins: results from the western Barents Sea, J. Geophys. Res., 104, 15293, doi:10.1029/1998JB900022, 1999.
Breivik, A. J., Mjelde, R., Grogan, P., Shimamura, H., Murai, Y., and Nishimura, Y.: Crustal structure and transform margin development south of Svalbard based on ocean bottom seismometer data, Tectonophysics, 369, 37–70, doi:10.1016/S0040-1951(03)00131-8, 2003.
Breivik, A. J., Mjelde, R., Grogan, P., Shimamura, H., Murai, Y., and Nishimura, Y.: Caledonide development offshore–onshore Svalbard based on ocean bottom seismometer, conventional seismic, and potential field data, Tectonophysics, 401, 79–117, doi:10.1016/j.tecto.2005.03.009, 2005.
Cherepanova, Y., Artemieva, I. M., Thybo, H., and Chemia, Z.: Crustal structure of the Siberian craton and the West Siberian basin: an appraisal of existing seismic data, Tectonophysics, 609, 154–183, doi:10.1016/j.tecto.2013.05.004, 2013.
Clark, S. A., Glorstad-Clark, E., Faleide, J. I., Schmid, D., Hartz, E. H., and Fjeldskaar, W.: Southwest Barents Sea rift basin evolution: comparing results from backstripping and time-forward modelling, Basin Res., 25, 1–17, doi:10.1111/bre.12039, 2013.
Cloetingh, S. and Burov, E.: Lithospheric folding and sedimentary basin evolution: a review and analysis of formation mechanisms, Basin Res., 23, 257–290, doi:10.1111/j.1365-2117.2010.00490.x, 2011.
Cocks, L. R. M. and Torsvik, T. H.: Baltica from the late Precambrian to mid-Palaeozoic times: the gain and loss of a terrane's identity, Earth-Sci. Rev., 72, 39–66, doi:10.1016/j.earscirev.2005.04.001, 2005.
Czuba, W., Grad, M., Mjelde, R., Guterch, A., Libak, A., Krüger, F., Murai, Y., and Schweitzer, J.: Continent–ocean-transition across a trans-tensional margin segment: off Bear Island, Barents Sea, Geophys. J. Int., 184, 541–554, doi:10.1111/j.1365-246X.2010.04873.x, 2011.
Dick, H. J. B., Lin, J., and Schouten, H.: An ultraslow-spreading class of ocean ridge., Nature, 426, 405–412, doi:10.1038/nature02128, 2003.
Dimakis, P., Braathen, B. I., Faleide, J. I., Elverhøi, A., and Gudlaugsson, S. T.: Cenozoic erosion and the preglacial uplift of the Svalbard–Barents Sea region, Tectonophysics, 300, 311–327, doi:10.1016/S0040-1951(98)00245-5, 1998.

SED
6, 1579–1624, 2014

Dörr, N., Lisker, F., Clift, P. D., Carter, A., Gee, D. G., Tebenkov, A. M., and Spiegel, C.: Late Mesozoic–Cenozoic exhumation history of northern Svalbard and its regional significance: constraints from apatite fission track analysis, Tectonophysics, 514–517, 81–92, doi:10.1016/j.tecto.2011.10.007, 2012.

Dörr, N., Clift, P. D., Lisker, F., and Spiegel, C.: Why is Svalbard an island? Evidence for two-stage uplift, magmatic underplating, and mantle thermal anomalies, Tectonics, 32, 473–486, doi:10.1002/tect.20039, 2013.

Drachev, S. and Saunders, A.: The Early Cretaceous Arctic LIP: its geodynamic setting and implications for Canada Basin opening, in: Proceedings of the Int. Conf. Arct. Margins, 4th, Anchorage, 216–223, available at: http://www.diva-portal.org/smash/get/diva2:207900/FULLTEXT01.pdf#page=226 (last access: 13 May 2014), 2006.

Dubinin, E. P., Kokhan, A. V., and Sushchevskaya, N. M.: Tectonics and magmatism of ultraslow spreading ridges, Geotectonics, 47, 131–155, doi:10.1134/S0016852113030023, 2013.

Engen, Ø., Faleide, J. I., and Dyreng, T. K.: Opening of the Fram Strait gateway: a review of plate tectonic constraints, Tectonophysics, 450, 51–69, doi:10.1016/j.tecto.2008.01.002, 2008.

Faleide, J. I., Vågnes, E., and Gudlaugsson, S. T.: Late Mesozoic–Cenozoic evolution of the south-western Barents Sea in a regional rift-shear tectonic setting, Mar. Petrol. Geol., 10, 186–214, doi:10.1016/0264-8172(93)90104-Z, 1993.

Faleide, J. I., Solheim, A., Fiedler, A., Hjelstuen, B. O., Andersen, E. S., and Vanneste, K.: Late Cenozoic evolution of the western Barents Sea–Svalbard continental margin, Glob. Planet. Change, 12, 53–74, doi:10.1016/0921-8181(95)00012-7, 1996.

Faleide, J., Tsikalas, F., and Breivik, A.: Structure and evolution of the continental margin off Norway and the Barents Sea, Episodes, 31, 82–91, 2008.

Fischer, K. M., Ford, H. A., Abt, D. L., and Rychert, C. A.: The lithosphere–asthenosphere boundary, Annu. Rev. Earth Pl. Sci., 38, 551–575, doi:10.1146/annurev-earth-040809-152438, 2010.

Gac, S., Huismans, R. S., Podladchikov, Y. Y., and Faleide, J. I.: On the origin of the ultradeep East Barents Sea basin, J. Geophys. Res., 117, B04401, doi:10.1029/2011JB008533, 2012.

Gac, S., Huismans, R. S., Simon, N. S. C., Podladchikov, Y. Y., and Faleide, J. I.: Formation of intracratonic basins by lithospheric shortening and phase changes: a case study from the ultra-deep East Barents Sea basin, Terra Nova, 25, 459–464, doi:10.1111/ter.12057, 2013.

Gee, D., Beliakova, L., and Pease, V.: New, single zircon (Pb-evaporation) ages from Vendian intrusions in the basement beneath the Pechora Basin, northeastern Baltica, Polarforschung, 1998 (February 1999), 161–170, available at: http://epic.awi.de/28429/1/Polarforsch1998_20.pdf (last access: 19 December 2012), 2000.
Gee, D., Bogolepova, O. K., and Lorenz, H.: The Timanide, Caledonide and Uralide orogens in the Eurasian high Arctic, and relationships to the palaeo-continents Laurentia, Baltica and Siberia, Geol. Soc. Lond. Mem., 32, 507–520, doi:10.1144/GSL.MEM.2006.032.01.31, 2006.
Gernigon, L. and Brönner, M.: Late Palaeozoic architecture and evolution of the southwestern Barents Sea: insights from a new generation of aeromagnetic data, J. Geol. Soc. London, 169, 449–459, doi:10.1144/0016-76492011-131, 2012.
Gernigon, L., Brönner, M., Roberts, D., Olesen, O., Nasuti, A., and Yamasaki, T.: Crustal and basin evolution of the southwestern Barents Sea: from Caledonian orogeny to continental breakup, Tectonics, 33, 347–373, doi:10.1002/2013TC003439, 2014.
Glørstad-Clark, E., Faleide, J. I., Lundschien, B. A., and Nystuen, J. P.: Triassic seismic sequence stratigraphy and paleogeography of the western Barents Sea area, Mar. Petrol. Geol., 27, 1448–1475, doi:10.1016/j.marpetgeo.2010.02.008, 2010.
Glørstad-Clark, E., Clark, S. A., Faleide, J. I., Bjørkesett, S. S., Gabrielsen, R. H., and Nystuen, J. P.: Basin dynamics of the Loppa High area, SW Barents Sea: a history of complex vertical movements in an epicontinental basin, Ph.D. thesis, 93–147, 2011.
Green, P. and Duddy, I.: Synchronous exhumation events around the Arctic including examples from Barents Sea and Alaska North Slope, Petrol. Geol., 7, 633–644, doi:10.1144/0070633, 2010.
Gudlaugsson, S., Faleide, J. I., Johansen, S. E., and Breivik, A. J.: Late Palaeozoic structural development of the South-western Barents Sea, Mar. Petrol. Geol., 15, 73–102, doi:10.1016/S0264-8172(97)00048-2, 1998.
Gung, Y., Panning, M., and Romanowicz, B.: Global anisotropy and the thickness of continents, Nature, 422, 707–711, doi:10.1038/nature01559, 2003.
Hauser, J., Dyer, K. M., Pasyanos, M. E., Bungum, H., Faleide, J. I., Clark, S. A., and Schweitzer, J.: A probabilistic seismic model for the European Arctic, J. Geophys. Res., 116, 1–17, doi:10.1029/2010JB007889, 2011.

SED
6, 1579–1624, 2014

A lithosphere-scale structural model of the Barents Sea and Kara Sea region

P. Klitzke et al.

Heine, C., Dietmar Müller, R., Steinberger, B., and Torsvik, T. H.: Subsidence in intracontinental basins due to dynamic topography, Phys. Earth Planet. In., 171, 252–264, doi:10.1016/j.pepi.2008.05.008, 2008.

Henriksen, E., Bjornseth, H. M., Hals, T. K., Heide, T., Kiryukhina, T., Klovjan, O. S., Larssen, G. B., Ryseth, A. E., Ronning, K., Sollid, K., and Stoupakova, A.: Uplift and erosion of the greater Barents Sea: impact on prospectivity and petroleum systems, Geol. Soc. Lond. Mem., 35, 271–281, doi:10.1144/M35.17, 2011a.

Henriksen, E., Ryseth, A. E., Larssen, G. B., Heide, T., Ronning, K., Sollid, K., and Stoupakova, A. V.: Tectonostratigraphy of the greater Barents Sea: implications for petroleum systems, Geol. Soc. Lond. Mem., 35, 163–195, doi:10.1144/M35.10, 2011b.

Huang, P. Y. and Solomon, S. C.: Centroid depths of mid-ocean ridge earthquakes: dependence on spreading rate, J. Geophys. Res., 93, 13445, doi:10.1029/JB093iB11p13445, 1988.

Ivanova, N. M., Sakoulina, T. S., and Roslov, Y. V.: Deep seismic investigation across the Barents–Kara region and Novozemelskiy Fold Belt (Arctic Shelf), Tectonophysics, 420, 123–140, doi:10.1016/j.tecto.2006.01.011, 2006.

Ivanova, N. M., Sakulina, T. S., Belyaev, I. V., Matveev, Y. I., and Roslov, Y. V.: Depth model of the Barents and Kara seas according to geophysical surveys results, Geol. Soc. Lond. Mem., 35, 209–221, doi:10.1144/M35.12, 2011.

Jakobsson, M., Mayer, L., Coakley, B., Dowdeswell, J. A., Forbes, S., Fridman, B., Hodnesdal, H., Noormets, R., Pedersen, R., Rebesco, M., Schenke, H. W., Zarayskaya, Y., Accettella, D., Armstrong, A., Anderson, R. M., Bienhoff, P., Camerlenghi, A., Church, I., Edwards, M., Gardner, J. V., Hall, J. K., Hell, B., Hestvik, O., Kristoffersen, Y., Marcussen, C., Mohammad, R., Mosher, D., Nghiem, S. V., Pedrosa, M. T., Travaglini, P. G., and Weatherall, P.: The International Bathymetric Chart of the Arctic Ocean (IBCAO) version 3, Geophys. Res. Lett., 39, L12609, doi:10.1029/2012GL052219, 2012.

Japsen, P., Green, P. F., Bonow, J. M., Rasmussen, E. S., Chalmers, J. A., and Kjennerud, T.: Episodic uplift and exhumation along North Atlantic passive margins: implications for hydrocarbon prospectivity, Geol. Soc. London, Petol. Geol. Conf. Ser., 7, 979–1004, doi:10.1144/0070979, 2010.

Johansen, S. E.: Hydrocarbon potential in the Barents Sea region: play distribution and potential, Arct. Geol. Pet. Potential, 2, 273–320, 1992.

Karato, S.: On the origin of the asthenosphere, Earth Planet. Sc. Lett., 321, 95–103, doi:10.1016/j.epsl.2012.01.001, 2012.

Khutorskoi, M. D., Viskunova, K. G., Podgornykh, L. V., Suprunenko, O. I., and Akhmedzyanov, V. R.: A temperature model of the crust beneath the Barents Sea: investigations along geotraverses, Geotectonics, 42, 125–136, doi:10.1134/S0016852108020039, 2008.

Knies, J., Matthiessen, J., Vogt, C., Laberg, J. S., Hjelstuen, B. O., Smelror, M., Larsen, E., Andreassen, K., Eidvin, T., and Vorren, T. O.: The Plio-Pleistocene glaciation of the Barents Sea–Svalbard region: a new model based on revised chronostratigraphy, Quaternary Sci. Rev., 28, 812–829, doi:10.1016/j.quascirev.2008.12.002, 2009.

Koptev, A. I. and Ershov, A. V.: Thermal thickness of the Earth's lithosphere: a numerical model, Moscow Univ. Geol. Bull., 66, 323–330, doi:10.3103/S014587521105005X, 2011.

Kostyuchenko, S., Sapozhnikov, R., Egorkin, A., Gee, D. G., Berzin, R., and Solodilov, L.: Crustal structure and tectonic model of northeastern Baltica, based on deep seismic and potential field data, Geol. Soc. Lond. Mem., 32, 521–539, doi:10.1144/GSL.MEM.2006.032.01.32, 2006.

Levshin, A. L., Schweitzer, J., Weidle, C., Shapiro, N. M., and Ritzwoller, M. H.: Surface wave tomography of the Barents Sea and surrounding regions, Geophys. J. Int., 170, 441–459, doi:10.1111/j.1365-246X.2006.03285.x, 2007.

Libak, A., Eide, C. H., Mjelde, R., Keers, H., and Flüh, E. R.: From pull-apart basins to ultraslow spreading: results from the western Barents Sea Margin, Tectonophysics, 514–517, 44–61, doi:10.1016/j.tecto.2011.09.020, 2012.

Ljones, F., Kuwano, A., Mjelde, R., Breivik, A., Shimamura, H., Murai, Y., and Nishimura, Y.: Crustal transect from the North Atlantic Knipovich Ridge to the Svalbard Margin west of Hornsund, Tectonophysics, 378, 17–41, doi:10.1016/j.tecto.2003.10.003, 2004.

Lorenz, H., Männik, P., Gee, D., and Proskurnin, V.: Geology of the Severnaya Zemlya Archipelago and the North Kara Terrane in the Russian high Arctic, Int. J. Earth Sci., 97, 519–547, doi:10.1007/s00531-007-0182-2, 2007.

Maher, J. and Harmon, D.: Manifestations of the Cretaceous High Arctic Large Igneous Province in Svalbard, J. Geol., 109, 91–104, doi:10.1086/317960, 2001.

Malyshev, N. A., Nikishin, V. A., Nikishin, A. M., Obmetko, V. V., Martirosyan, V. N., Kleshchina, L. N., and Reydik, Y. V.: A new model of the geological structure and evolution of the North Kara Sedimentary Basin, Dokl. Earth Sci., 445, 791–795, doi:10.1134/S1028334X12070057, 2012a.

SED

6, 1579–1624, 2014

A lithosphere-scale structural model of the Barents Sea and Kara Sea region

P. Klitzke et al.

Malyshev, N. A., Nikishin, V. A., Obmetko, V. V., Ikhsanov, B. I., Reydik, Y. V., Sitar, K. A., and Shapabaeva, D. S.: Geological Structure and Petroleum System of South Kara Basin, Saint Petersburg, 2012b.

Marello, L., Ebbing, J., and Gernigon, L.: Basement inhomogeneities and crustal setting in the Barents Sea from a combined 3D gravity and magnetic model, Geophys. J. Int., 193, 557–584, doi:10.1093/gji/ggt018, 2013.

McKenzie, D. and Priestley, K.: The influence of lithospheric thickness variations on continental evolution, Lithos, 102, 1–11, doi:10.1016/j.lithos.2007.05.005, 2008.

Minakov, A., Faleide, J. I., Glebovsky, V. Y., and Mjelde, R.: Structure and evolution of the northern Barents-Kara Sea continental margin from integrated analysis of potential fields, bathymetry and sparse seismic data, Geophys. J. Int., 188, 79–102, doi:10.1111/j.1365-246X.2011.05258.x, 2012a.

Minakov, A., Mjelde, R., Faleide, J. I., Flueh, E. R., Dannowski, A., and Keers, H.: Mafic intrusions east of Svalbard imaged by active-source seismic tomography, Tectonophysics, 518, 106–118, doi:10.1016/j.tecto.2011.11.015, 2012b.

Nikishin, A., Ziegler, P., Abbott, D., Brunet, M.-F., and Cloetingh, S.: Permo–Triassic intraplate magmatism and rifting in Eurasia: implications for mantle plumes and mantle dynamics, Tectonophysics, 351, 3–39, doi:10.1016/S0040-1951(02)00123-3, 2002.

Nikishin, V. A., Malyshev, N. A., Nikishin, A. M., and Obmetko, V. V.: The late permian–triassic system of rifts of the South Kara sedimentary basin, Moscow Univ. Geol. Bull., 66, 377–384, doi:10.3103/S0145875211060093, 2011.

O'Leary, N., White, N., Tull, S., Bashilov, V., Kuprin, V., Natapov, L., and Macdonald, D.: Evolution of the TimanPechora and south Barents Sea basins, Geol. Mag., 141, 141–160, doi:10.1017/S0016756804008908, 2004.

Otto, S. and Bailey, R.: Tectonic evolution of the northern Ural Orogen, J. Geol. Soc. London, 152, 903–906, 1995.

Petrov, O., Sobolev, N., and Koren, T.: Palaeozoic and Early Mesozoic evolution of the East Barents and Kara Seas sedimentary basins, Norweg. J. Geol., 88, 227–234, 2008.

Piskarev, A. and Shkatov, M.: Sedimentary Basins of the Barents and Kara Seas, Development, Elsevier, 2012.

Priestley, K. and McKenzie, D.: The thermal structure of the lithosphere from shear wave velocities, Earth Planet. Sci. Lett., 244, 285–301, doi:10.1016/j.epsl.2006.01.008, 2006.

SED
6, 1579–1624, 2014

Puchkov, V. N.: The evolution of the Uralian orogen, Geol. Soc. London, Spec. Publ., 327, 161–195, doi:10.1144/SP327.9, 2009.
Reichow, M. K., Saunders, A. D., White, R. V., Al'Mukhamedov, A. I., and Medvedev, A. Y.: Geochemistry and petrogenesis of basalts from the West Siberian Basin: an extension of the Permo–Triassic Siberian Traps, Russia, Lithos, 79, 425–452, doi:10.1016/j.lithos.2004.09.011, 2005.
Ritzmann, O. and Faleide, J. I.: Caledonian basement of the western Barents Sea, Tectonics, 26, 1–20, doi:10.1029/2006TC002059, 2007.
Ritzmann, O. and Faleide, J. I.: The crust and mantle lithosphere in the Barents Sea/Kara Sea region, Tectonophysics, 470, 89–104, doi:10.1016/j.tecto.2008.06.018, 2009.
Ritzmann, O., Jokat, W., Mjelde, R., and Shimamura, H.: Crustal structure between the Knipovich Ridge and the Van Mijenfjorden (Svalbard), Mar. Geophys. Res., 23, 379–401, doi:10.1023/B:MARI.0000018168.89762.a4, 2002.
Ritzmann, O., Jokat, W., Czuba, W., Guterch, A., Mjelde, R., and Nishimura, Y.: A deep seismic transect from Hovgård Ridge to northwestern Svalbard across the continental–ocean transition: a sheared margin study, Geophys. J. Int., 157, 683–702, doi:10.1111/j.1365-246X.2004.02204.x, 2004.
Ritzmann, O., Maercklin, N., Inge Faleide, J., Bungum, H., Mooney, W. D., and Detweiler, S. T.: A three-dimensional geophysical model of the crust in the Barents Sea region: model construction and basement characterization, Geophys. J. Int., 170, 417–435, doi:10.1111/j.1365-246X.2007.03337.x, 2007.
Roberts, D. and Siedlecka, A.: Timanian orogenic deformation along the northeastern margin of Baltica, Northwest Russia and Northeast Norway, and Avalonian–Cadomian connections, Tectonophysics, 352, 169–184, doi:10.1016/S0040-1951(02)00195-6, 2002.
Saunders, A. D., England, R. W., Reichow, M. K., and White, R. V.: A mantle plume origin for the Siberian traps: uplift and extension in the West Siberian Basin, Russia, Lithos, 79, 407–424, doi:10.1016/j.lithos.2004.09.010, 2005.
Sauter, D., Sloan, H., Cannat, M., Goff, J., Patriat, P., Schaming, M., and Roest, W. R.: From slow to ultra-slow: how does spreading rate affect seafloor roughness and crustal thickness?, Geology, 39, 911–914, doi:10.1130/G32028.1, 2011.
Scott, R. and Howard, J.: Offset and curvature of the Novaya Zemlya fold-and-thrust belt, Arctic Russia, Petrol. Geol., 7, 645–657, 2010.

SED
6, 1579–1624, 2014

Semprich, J., Simon, N. S. C., and Podladchikov, Y. Y.: Density variations in the thickened crust as a function of pressure, temperature, and composition, Int. J. Earth Sci., 99, 1487–1510, doi:10.1007/s00531-010-0557-7, 2010.
Shapiro, N. M. and Ritzwoller, M. H.: Monte-Carlo inversion for a global shear-velocity model of the crust and upper mantle, Geophys. J. Int., 151, 88–105, doi:10.1046/j.1365-246X.2002.01742.x, 2002.
Smelror, M., Petrov, O., Larssen, G., and Werner, S.: Geological history of the Barents Sea, Norges Geol., 2009.
Sobolev, P.: Cenozoic uplift and erosion of the Eastern Barents Sea – constraints from offshore well data and the implication for petroleum system modelling, Zeitschrift der Dtsch. Gesellschaft für Geowissenschaften, 163, 309–324, doi:10.1127/1860-1804/2012/0163-0323, 2012.
Steer, D. N., Knapp, J. H., Brown, L. D., Echtler, H. P., Brown, D. L., and Berzin, R.: Deep structure of the continental lithosphere in an unextended orogen: an explosive-source seismic reflection profile in the Urals (Urals Seismic Experiment and Integrated Studies (URSEIS 1995)), Tectonics, 17, 143–157, doi:10.1029/97TC03056, 1998.
Stoupakova, A. V., Henriksen, E., Burlin, Y. K., Larsen, G. B., Milne, J. K., Kiryukhina, T. A., Golynchik, P. O., Bordunov, S. I., Ogarkova, M. P., and Suslova, A. A.: The geological evolution and hydrocarbon potential of the Barents and Kara shelves, Geol. Soc. Lond. Mem., 35, 325–344, doi:10.1144/M35.21, 2011.
Turcotte, D. L. and Schubert, G.: Geodynamics, Cambridge University Press, 2002.
Voss, M. and Jokat, W.: Continent-ocean transition and voluminous magmatic underplating derived from *P*-wave velocity modelling of the East Greenland continental margin, Geophys. J. Int., 170, 580–604, doi:10.1111/j.1365-246X.2007.03438.x, 2007.
Voss, M., Schmidt-Aursch, M. C., and Jokat, W.: Variations in magmatic processes along the East Greenland volcanic margin, Geophys. J. Int., 177, 755–782, doi:10.1111/j.1365-246X.2009.04077.x, 2009.
Vyssotski, A. V., Vyssotski, V. N., and Nezhdanov, A. A.: Evolution of the West Siberian Basin, Mar. Petrol. Geol., 23, 93–126, doi:10.1016/j.marpetgeo.2005.03.002, 2006.
Worsley, D.: The post-Caledonian development of Svalbard and the western Barents Sea, Polar Res., 27, 298–317, doi:10.1111/j.1751-8369.2008.00085.x, 2008.

SED
6, 1579–1624, 2014

Table A1. Database.

Horizon	Reference	Covered Region
Bathymetry	Jakobsson et al. (2012)	Entire study area
Earliest Eocene	Faleide et al. (1996)	Norwegian-Greenland Sea
	Fielder and Faleide (1996)	Norwegian-Greenland Sea
	Hjuelstuen et al. (1996)	Norwegian-Greenland Sea
	Engen et al. (2006)	Eurasia Basin
	Engen et al. (2009)	Eurasia Basin
	Glebosvki et al. (2006)	Eurasia Basin
	Gramberg et al. (2001)	Eurasia Basin
Mid-Cretaceous	Faleide et al. (1993a, b)	SW Barents Sea
	Brekhuntsov et al. (2011)	Southern Kara Sea–West Siberian Basin
Mid-Jurassic	Brekhuntsov et al. (2011)	Southern Kara Sea
	Faleide et al. (1993a, b)	SW Barents Sea
	Johansen et al. (1993)	Barents Sea
	Kontorovich et al. (2010)	Southern Kara Sea
	Norwegian Petroleum Directorate	Southern Kara Sea
	Piskarev and Shkatov (2012)	Eastern Barents and Kara Seas
Mid-Permian	Brekhuntsov et al. (2011)	Southern Kara Sea
	Henriksen et al. (2011)	Barents Sea
	Ivanova et al. (2011)	Barents and Kara Sea
	Johansen et al. (1993)	Barents Sea
	Khutorskoi et al. (2008)	Barents Sea
	Nikishin et al. (2011)	Southern Kara Sea
	Piskarev and Shkatov (2012)	Eastern Barents and Kara Seas
Top Crystalline Crust	Aplonov et al. (1996)	Eastern Barents and Kara Seas
	Drachev et al. (2011)	Eastern Barents and Kara Seas
	Gramberg et al. (2001)	Western Barents Sea
	Hauser et al. (2011)	Euopean Arctic
	Ivanova et al. (2011)	Barents and Kara Seas
	Johansen et al. (1993)	Barents Sea
	Myklebust (1994)	Barents Sea
	Ritzmann et al. (2006)	Barents Sea
	Skillbrei et al. (1991)	Barents Sea
Moho	Aplonov et al. (1996)	Eastern Barents–Kara Seas
	Dahl-Jensen et al. (2003)	NE Greenland
	Hauser et al. (2011)	European Arctic
	Ivanova et al. (2011)	Barents Sea
	Kostyuchenko et al. (2006)	Eastern Barents and Kara Seas
	Minakov et al. (2012)	Northern Barents Sea
	Ritzmann et al. (2006)	Barents Sea
Lithosphere–Asthenosphere Boundary	Levshin et al. (2007)	Barents Sea
	Shapiro and Ritzwoller (2002)	Kara Sea
	Kumar et al. (2005)	NE Greenland
	Zhang and Lay (1999)	Oceanic Domain

SED
6, 1579–1624, 2014

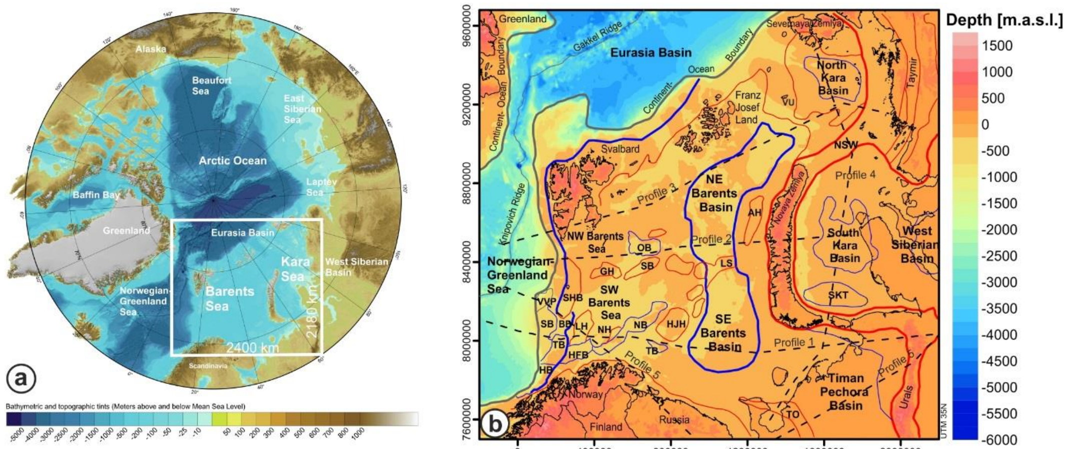

Figure 1. (a) Overview Map. The white rectangle encloses the extent of the 3-D structural model. **(b)** Superimposed Bathymetry/topography (IBCAO 3.0; Jakobsson et al., 2012) with outlines of structural highs (red) and lows (blue). The stippled lines mark the position of five representative profiles (see Fig. 6) crossing most prominent geological provinces. (AH) – Admiralty High; (BB) – Bjørnøya Basin; (GH) – Gardarbanken High; (HFB) – Hammerfest Basin; (HB) – Harstad Basin; (HJH) – Hjalmar Johansen High; (LH) – Loppa High; (LS) – Ludlov Saddle; (NB) – Nordkapp Basin; (NH) – Norsel High; (NSW) – North Siberian Weir; (OB) – Olga Basin; (SB) – Sørvestsnaget Basin; SH) – Sentralbakken High; (SKT) – South Kara Trough; (SHB) – Stappen High with Bjørnøya Island; (TB) – Tiddlybanken Basin; (TO) – Timan Orogen; (TB) – Tromsø Basin; (VU) Vize-Ushakov Rise; (VVP) – Vestbakken Volcanic Province

SED
6, 1579–1624, 2014

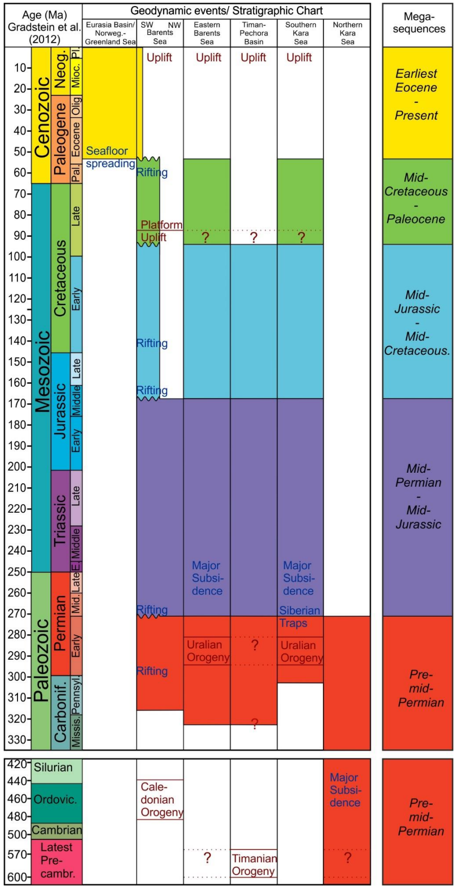

Figure 2. Stratigraphic megasequences resolved in the 3-D structural model in relation to regional tectonic events. Oldest sediments are preserved in the northern Kara Sea whereas Cenozoic deposits are present only in the southwesternmost Barents Sea and in the oceanic domain.

SED

6, 1579–1624, 2014

A lithosphere-scale structural model of the Barents Sea and Kara Sea region

P. Klitzke et al.

Title Page
Abstract | Introduction
Conclusions | References
Tables | Figures
◀| |▶
◀ ▶
Back | Close
Full Screen / Esc
Printer-friendly Version
Interactive Discussion

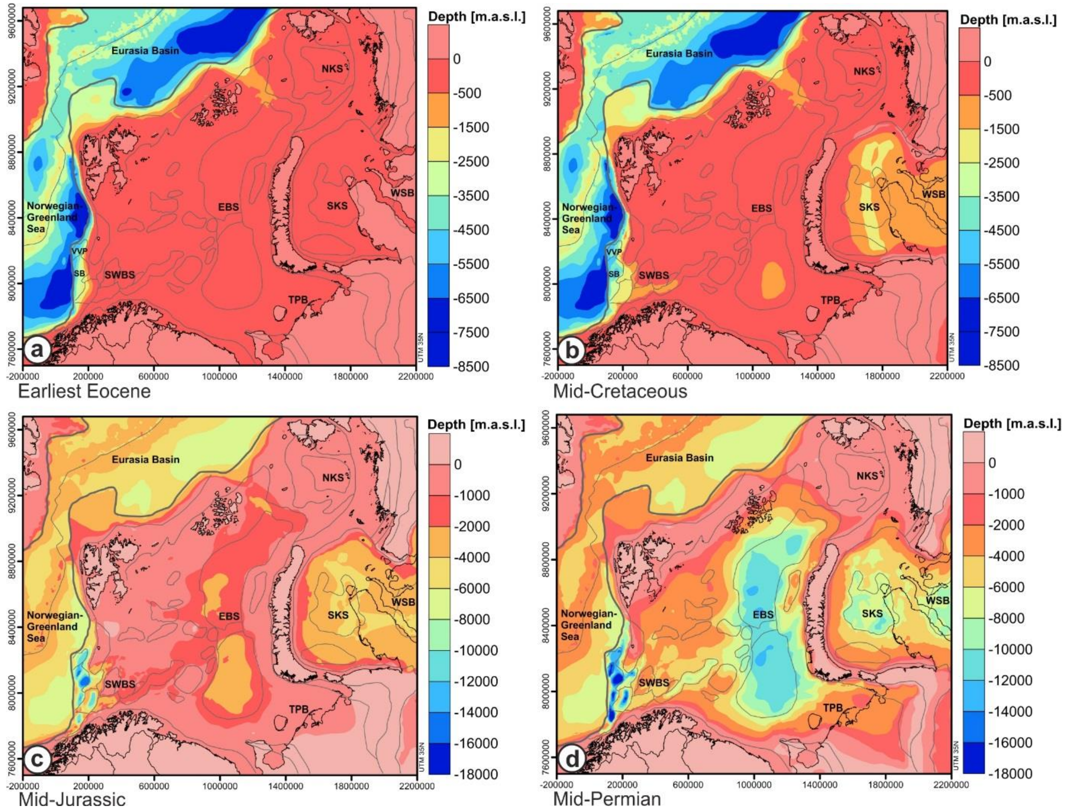

Figure 3. Depth to the four modelled megasequence boundaries: **(a)** Earliest Eocene **(b)** Mid-Cretaceous **(c)** Mid-Jurassic **(d)** Mid-Permian. The grey lines delineate structural features in the study area (for legend see Fig. 1b). The Earliest Eocene surface equals the Top Crystalline Basement in the oceanic domain. See Table A1 for database.

SED
6, 1579–1624, 2014

Title Page
Abstract | Introduction
Conclusions | References
Tables | Figures
I◀ | ▶I
◀ | ▶
Back | Close
Full Screen / Esc
Printer-friendly Version
Interactive Discussion

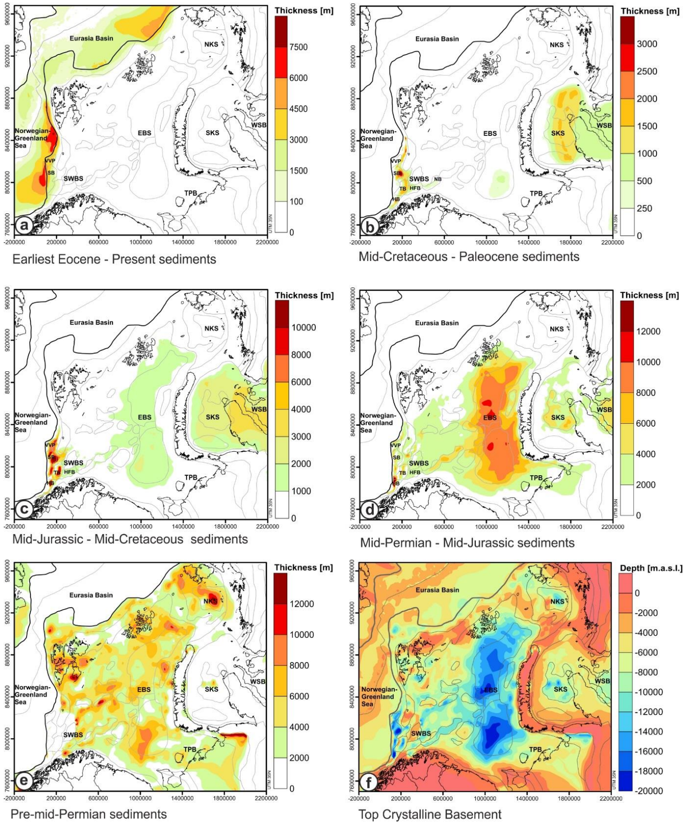

Figure 4. Thickness distribution of the megasequences and the depth to the top crystalline crust: **(a)** Earliest Eocene–Present; **(b)** Mid-Cretaceous–Paleocene; **(c)** Mid-Jurassic–Mid-Cretaceous; **(d)** Mid-Permian–Mid-Jurassic; **(e)** Pre-mid-Permian; **(f)** Depth Top Crystalline Basement. The grey lines delineate structural features in the study area (for legend see Fig. 1b). See Table A1 for database.

SED
6, 1579–1624, 2014
A lithosphere-scale structural model of the Barents Sea and Kara Sea region
P. Klitzke et al.

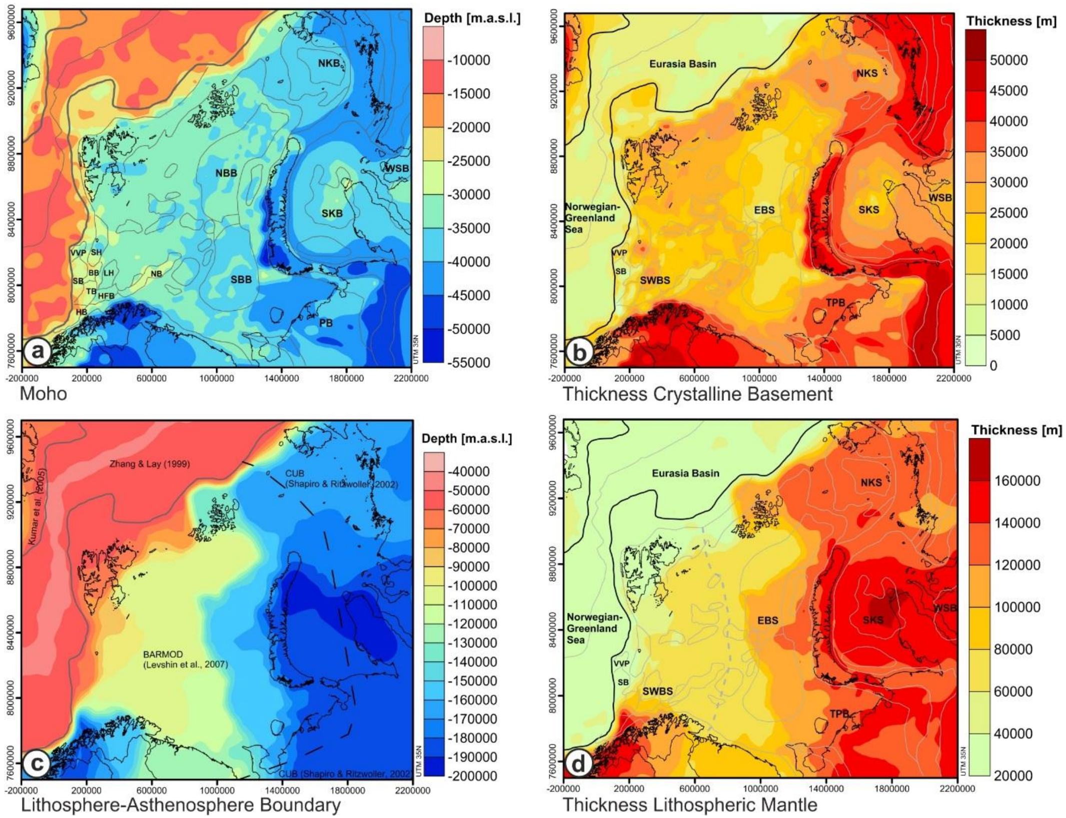

Figure 5. Structure of the deeper crust and the upper mantle: **(a)** depth to the Moho; **(b)** thickness of the crystalline crust; **(c)** depth to the lithosphere–asthenosphere boundary (LAB); **(d)** thickness of the lithospheric mantle.

SED
6, 1579–1624, 2014

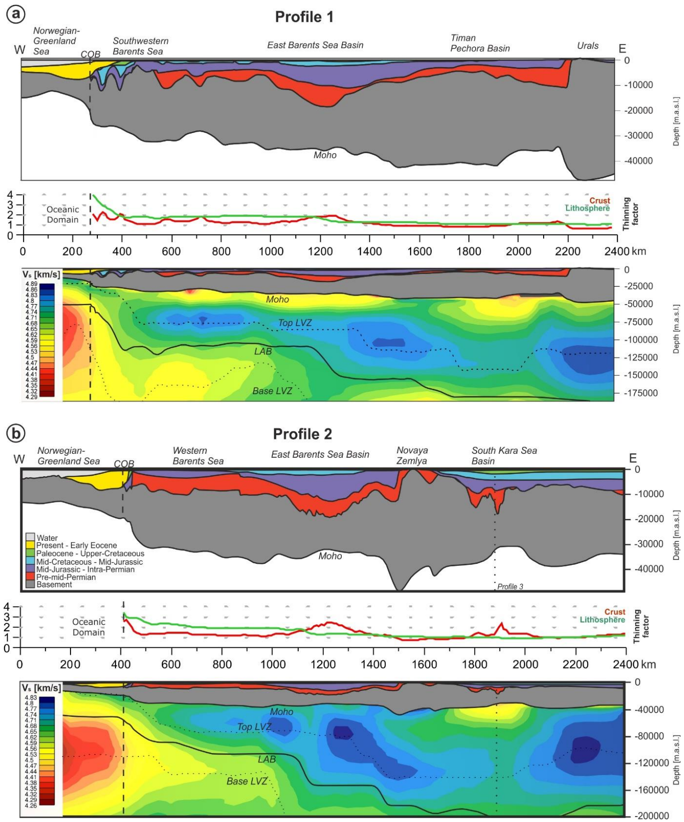

Figure 6. Five profiles illustrating the main geological units and the velocity structure (BARMOD, CUB1.0) on crustal and lithosphere-scale (for location see Fig. 1b; LVZ – low velocity zone). The thinning factors are calculated with reference values of 32 km and 200 km for the crystalline basement and the lithospheric mantle, respectively. Vertical exaggeration of the crustal-scale profiles: 5×, exaggeration of the lithosphere-scale profiles: 3×.

SED
6, 1579–1624, 2014

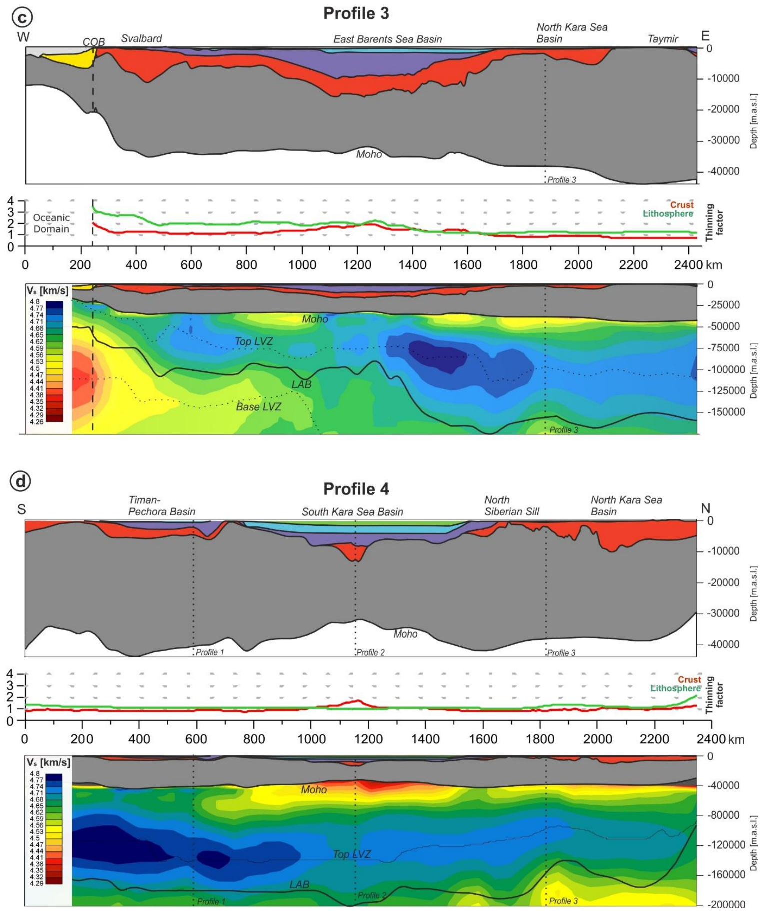

Figure 6. Continued.

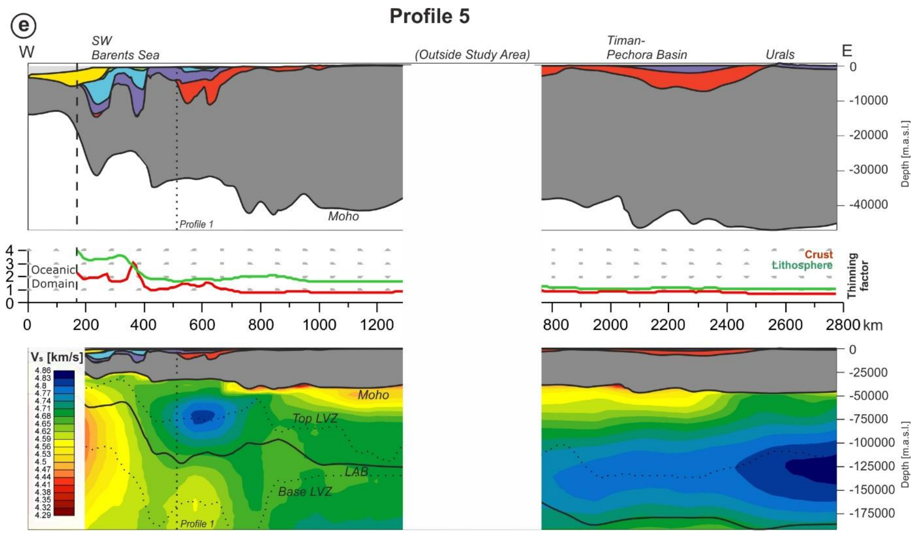

Figure 6. Continued.

SED
6, 1579–1624, 2014

A lithosphere-scale structural model of the Barents Sea and Kara Sea region

P. Klitzke et al.

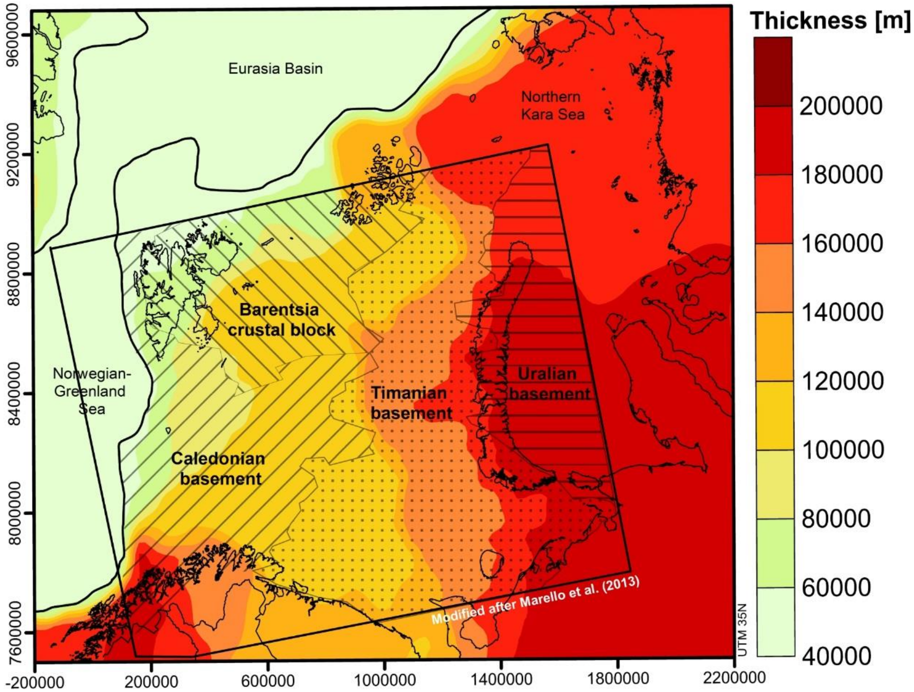

Figure 7. The simplified subdivision of basement terranes after Marello et al. (2013) plotted on the total thickness of the lithosphere. The black frame marks the model extent of Marello et al. (2013).

SED
6, 1579–1624, 2014

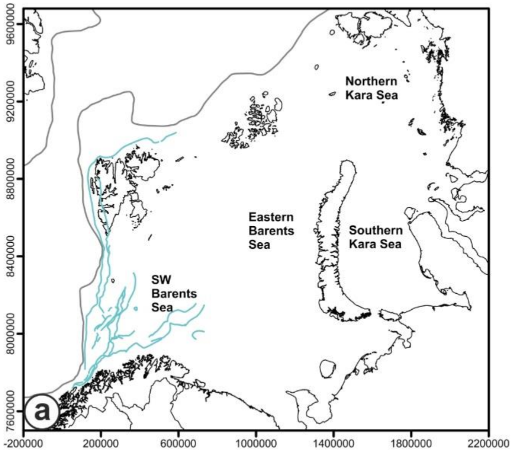

Figure B1. Mesozoic **(a)** and Paleozoic **(b)** fault-sets (Faleide et al., 1993; Gudlaugsson et al., 1998) which cover the western Barents Sea and were used as vertical interpolation barriers for the respective megasequence boundaries.

SED
6, 1579–1624, 2014